

## An Analytical Solution of the Ideal-Fluid Thermocline\*

RUI XIN HUANG

*Woods Hole Oceanographic Institution, Woods Hole, Massachusetts*

(Manuscript received 7 February 2000, in final form 13 February 2001)

### ABSTRACT

An exact analytical solution for the ideal-fluid thermocline is discussed. The solution is calculated from the specified functional relations: for the ventilated thermocline it is a linear functional relation between the potential thickness and the Bernoulli function, and for the unventilated thermocline the potential thickness is a constant. The solution satisfies the most important dynamic constraints—the Sverdrup relation and other boundary conditions. For any given Ekman pumping field, the surface density that satisfies the a priori specified potential thickness function is calculated as part of the solution. Climate variability induced by surface cooling/heating is inferred from the construction of the Green function. It is shown that for the model based on the special functional form discussed in this paper, the cooling-induced anomaly is in the form of the second dynamic thermocline mode that has a zero-crossing in the middle of the thermocline, resembling the second baroclinic mode defined in the classic stability analysis.

### 1. Introduction

The main thermocline or pycnocline in the subtropical basins is one of the most prominent features in the oceans. The existence of the main thermocline has been known for more than a century, and over the past decades thermocline theory has been developed in order to explain its structure and the associated circulation.

From the very beginning of the development, there have been two approaches to this problem. In 1959, two papers were published side by side in *Tellus*. Robinson and Stommel (1959) proposed a theory of the thermocline in which the vertical diffusion plays a vital role. In this approach, the main thermocline is viewed as an internal density front or internal thermal boundary layer, thus the vertical diffusion should be retained. The early development along this line was summed up in the comprehensive review by Veronis (1969). The most challenging difficulty associated with this approach is that nobody knows how to formulate suitable boundary value problems for the corresponding nonlinear equation system, much less how to find the solutions to this problem. In order to overcome such difficulty, many similarity solutions have been sought and discussed. The major disadvantage of the similarity solutions is that

they do not satisfy important boundary conditions, such as the Sverdrup constraint.

On the other hand, Welander (1959) proposed an ideal-fluid theory for the thermocline. From the beginning, the basic equations for the thermocline seemed so naively simple that many people believed that they could be solved easily, so most people did not want to spend time working on the seemingly incomplete ideal-fluid thermocline theory, except Welander who also published another very influential paper on the ideal-fluid thermocline (Welander 1971).

The basic ideas for the ideal-fluid thermocline can be shown clearly in terms of density coordinates and the Bernoulli function

$$B = p + \rho g z, \quad (1)$$

where  $p$  is pressure,  $\rho$  is density,  $g$  is gravity, and  $z$  is the vertical coordinate. Differentiating this equation leads to

$$B_\rho = g z, \quad (2)$$

$$B_{\rho\rho} = -\frac{fg}{Q}, \quad (3)$$

where  $f = 2\Omega \sin \phi$  is the Coriolis parameter ( $\Omega$  is the angular velocity of the earth's rotation,  $\phi$  is the latitude), and

$$Q = -f\rho_z \quad (4)$$

is the PV. It is readily shown that three quantities, density  $\rho$ , Bernoulli function  $B$ , and PV  $Q$ , are conserved along streamlines. Thus, there is a relation between them

\* Woods Hole Oceanographic Institution Contribution Number 10165.

Corresponding author address: Dr. Rui Xin Huang, Department of Physical Oceanography, Woods Hole Oceanographic Institution, Woods Hole, MA 02543.  
E-mail: rhnang@whoi.edu

$$Q = Q(\rho, B). \quad (5)$$

For a given relation (5) the solution can be found from (3) or (4), plus suitable boundary conditions.

Assuming (Welander 1971)

$$Q = -(\alpha\rho + \beta B + \gamma), \quad (6)$$

Eq. (4) leads to a second-order ode in  $z$  coordinates

$$f\rho_{zz} = (\alpha + \beta gz)\rho_z. \quad (7)$$

The first integration of this equation leads to

$$\rho_z = C(\lambda, \phi)e^{(\alpha z + \beta gz^2/2)/f}, \quad (8)$$

where  $C(\lambda, \phi)$  is a constant depending on the longitude  $\lambda$  and latitude  $\phi$ , and its integration leads to an analytical solution

$$\rho = \rho_0(\lambda, \phi) + C(\lambda, \phi) \int_0^z \exp\left[-\left(\frac{\xi + z_0}{D_0}\right)\frac{1}{\sin\phi}\right] d\xi, \quad (9)$$

where  $\rho_0(\lambda, \phi)$  and  $C(\lambda, \phi)$  can be determined by matching the density at the upper and lower boundaries, which were chosen at  $z = 0$  and  $z \rightarrow -\infty$ ;  $z_0$  and  $D_0$  are constants specified a priori. For details of this solution see Welander (1971).

Although this is the first elegant solution for the ideal-fluid thermocline, and thus has been cited in many text books, it has some major defects: the solution satisfies neither the Sverdrup relation nor the eastern boundary condition, and the lower boundary is set at  $z = -\infty$ . Since the Sverdrup constraint is the most important constraint, thermocline solutions that do not satisfy the Sverdrup relation are less meaningful dynamically. In this sense, Welander's original solution is also incomplete. It turned out that the wind-driven gyre consists of many regimes that are dynamically different; thus, treating the wind-driven gyre with a single PV functional relation, as proposed by Welander, is not a good choice.

During the 1960s, similarity solutions remained the mainstream in thermocline theory. However, the limitation of the similarity approach became clear, and there was a period of relatively low activity in the 1970s. Beginning in the early 1980s there were major breakthroughs in the theory of the dynamic structure of the wind-driven gyre, including the PV homogenization theory by Rhines and Young (1982) and the ventilated thermocline by Luyten et al. (1983). According to these new theories, the wind-driven gyre includes several regions with different dynamics: the ventilated thermocline where PV is set at the surface, the unventilated thermocline where PV is homogenized, the shadow zone near the eastern boundary, and the pool region near the western boundary. These new theories were combined and extended to a theory of the wind-driven gyre in the continuously stratified oceans by Huang (1988). The dynamic role of the mixed layer, excluded from the early

theories, was incorporated into the thermocline theory (e.g., Huang 1990; Pedlosky and Robbins 1991; Williams 1991). The progress made during the past two decades was reviewed by Huang (1991) and Pedlosky (1996).

Tracer release experiments in the 1990s provided strong support for the ideal-fluid thermocline theory because it was found that diapycnal mixing is very small in the main thermocline, on the order of  $0.1 \text{ cm}^2 \text{ s}^{-1}$ . Thus, to a very good approximation the structure of the thermocline and the wind-driven circulation can be treated as ideal-fluid motion. It is also very important to notice that diapycnal mixing is very small, but not infinitesimal; thus, the theoretical limit of letting mixing go to zero does not apply to the world oceans.

The basic assumption in the ideal-fluid thermocline theory is to treat the wind-driven circulation as a (finite amplitude) perturbation to a specified background stratification [or Potential vorticity (PV) distribution in density coordinates]. Thus, a small but finite rate of mixing is included in the zero-order PV–density structure; however, there is no mixing in the first-order solution. Therefore, the ideal-fluid thermocline theory does not incorporate a nonzero mixing, so it is different from the aforementioned theoretical limit of letting mixing go to zero.

A shortcoming of Welander's solution is that it does not satisfy the Ekman pumping condition. This is, however, an issue that can be readily reconciled by incorporating the Ekman pumping condition as an upper boundary condition for the model thermocline, as shown by Huang (1986). However, this solution is also incomplete because it does not satisfy a suitable lower boundary condition. At that time, however, it was unclear what the suitable lower boundary conditions for a continuously stratified model were, so it was also unclear how to apply the Sverdrup constraint to such a model.

The solution of the ideal-fluid thermocline for a continuously stratified ocean was formulated in terms of a two-point boundary value problem with a free boundary (the base of the wind-driven gyre) by Huang (1988). One of the most important features of the solution is that it satisfies the Sverdrup constraint and suitable boundary conditions along the eastern and lower boundaries. However, the solution of this boundary value problem has been limited to the finite difference discretization of the continuous formulation. Therefore, the structure of a truly continuous solution has remained unclear. In this study we will show that truly continuous solutions that satisfy the Sverdrup relation can be found.

During the past 20 years progress has also been made on thermocline theory emphasizing the dynamic role of vertical mixing. Based on the similarity approach, Salmon (1990) argued that in the limit of infinitely small diffusion, the thermocline should appear in the form of a density step function. The similarity approach to the thermocline has been pursued further by Salmon and Hollerbach (1991) and Hood and Williams (1996).

Both the ventilated thermocline and diffusive ther-

mocline theories represent idealizations of the thermocline circulation in the real world; thus, they both have limitations. For example, in the ideal-fluid thermocline theory, the dynamic role of vertical and horizontal mixing is implicitly included through the specification of PV for the unventilated thermocline. On the other hand, although vertical diffusion is included in the diffusive thermocline theory of the wind-driven gyres, horizontal mixing is excluded. Another major disadvantage of the diffusive thermocline is our inability to find solutions that can satisfy the Sverdrup constraint; thus, most solutions obtained so far do not provide us with the basinwide structure of the wind-driven gyre.

A major deficit of thermocline theories is the lack of the western boundary layer and recirculation. It is clear that in order to explain the structure of the wind-driven circulation, numerical models must be used in which the dynamic effects of horizontal mixing, the western boundary layer, and the recirculation are explicitly included. For example, Samelson and Vallis (1997) studied the thermocline structure in a closed basin and showed that, by using a small diapycnal mixing rate in the ocean interior, the thermocline does appear in two dynamic regimes, that is, the ventilated thermocline for the water entering from the surface layer in the subtropical basin due to Ekman pumping and the diffusive thermocline over the density range corresponding to the subpolar basin. In a more recent publication, Vallis (2000) went through a series of carefully designed numerical experiments based on a primitive equation model and showed that stratification below the ventilated thermocline is a result of global dynamics, involving the effect of wind forcing, geometry of the world oceans, and diffusion. In particular, his study indicated that the geometry of the Antarctic Circumpolar Current plays a subtle but important role in setting up the stratification at the middepth of the world oceans.

Although a simple analytical theory of the ideal-fluid thermocline cannot possibly explain the details of the wind-driven circulation, it does provide important insight into the fundamental structure of the circulation. With this limit in mind, we will concentrate on improving simple solutions for the thermocline. In section 2 we begin to examine a simple analytical solution of the ideal-fluid thermocline equation. Assuming a simple linear relation between the potential thickness and the Bernoulli function for the ventilated thermocline, plus a constant PV for the unventilated thermocline, a simple solution for the wind-driven gyre is obtained. The calculation of such a solution is reduced to solving a single nonlinear algebraic equation at each station. The most important characteristics of such a solution are: it satisfies the Sverdrup constraint, and its structure resembles the wind-driven gyres observed in the oceans. In section 3, we explore some extensions of this approach and show that our formulation can be easily extended and other solutions can be generated that resemble the observed features of the thermocline in the oceans.

Climate variability has become one of the main focuses in recent studies. The ideal-fluid thermocline theory has been used as the theoretical framework for the study of climate variability (e.g., Deser et al. 1996; Liu 1999; Schneider et al. 1999). Assuming that climate variability on decadal timescales can be treated as the difference between two quasi-steady states, climate variability can be inferred from models of the ideal-fluid thermocline, including the 2½-layer model (Huang and Pedlosky 1999), the 4½-layer model (Huang and Pedlosky 2000), and the continuous model (Huang 2000b). Since these models are not truly continuous, one cannot find the exact form of climate variability induced by a point source of buoyancy or Ekman pumping anomaly. Theoretically, climate variability due to anomalous surface forcing can be treated as the superposition of the influence due to an individual source; thus, the study of climate variability can be reduced to the study of the corresponding Green function. As will be shown in section 4, climate variability induced by cooling is likely to appear in the form of the second dynamic thermocline mode, which resembles the classic second baroclinic mode because of the existence of a zero crossing in the middle depth of the thermocline. Our main results are concluded in section 5.

## 2. A new analytical model for the ideal-fluid thermocline

A slightly different approach to the ideal-fluid thermocline is based on density coordinates, so the starting point is Eq. (3), instead of (4). For convenience, we will rewrite Eq. (3) in the following form

$$B_{\rho\rho} = -fgD, \quad (10)$$

where  $D = 1/Q = -z_\rho/f$  is the potential thickness, which is conserved along the streamlines. There are several simple choices that can be solved analytically.

### a. A linear functional relation

The linear functional relation is

$$D = a_0^2 B - b_0 \rho - c_0. \quad (11)$$

The reason for assuming a positive coefficient  $a_0^2$  is that in the subtropical basin interior the layer thickness increases westward. Thus, both  $B$  and  $D$  should increase westward. Introducing the new parameters

$$a = \sqrt{fg}a_0, \quad b = fgb_0, \quad c = fgc_0,$$

the general solution to this equation is

$$B = \frac{b}{a^2}[\rho + c_1 \cos a(\rho - \rho_c)] + \frac{c}{a^2}, \quad (12)$$

where  $c_1$  and  $\rho_c$  are two constants to be determined. In fact, Welander (1971) discussed the general solutions when  $D = F(aB + b\rho + c)$ , where  $F$  is an arbitrary function. Killworth (1987) also studied similar cases.

*b. A simple case with PV independent of density*

We consider the case when  $D$  linearly depends on  $B$ . In this study we assume that layer thickness is zero along the eastern boundary, so  $D = a_0^2 B$  is a simple choice. In addition, the potential thickness of the unventilated thermocline is assumed to be constant. The equation corresponding to (10) is

$$B_{\rho\rho} + a^2 B = 0, \tag{13}$$

where  $a = \sqrt{fga_0}$ .

The general solution for this equation that satisfies the upper boundary condition

$$B_\rho = 0, \text{ at } \rho = \rho_s \tag{14}$$

is

$$B = c_1 \cos a(\rho - \rho_s), \tag{15}$$

where  $\rho_s = \rho_s(\lambda, \phi)$  is the unknown sea surface density and  $c_1 = c_1(\lambda, \phi)$  is an integration constant that can be determined by the boundary conditions. This can be rewritten as

$$B = -\frac{\cos a(\rho - \rho_s)}{a \sin a\Delta\rho} B_{\rho,0}, \tag{16}$$

where  $\Delta\rho = \rho_0 - \rho_s$ ,  $B_{\rho,0} = dB/d\rho|_{\rho=\rho_0}$  ( $\rho_0$  is the density of the isopycnal that outcrops along the boundary between the subpolar and subtropical gyres, so it is the boundary that separates the ventilated thermocline from the unventilated thermocline). The corresponding first derivative is

$$B_\rho = \frac{\sin a(\rho - \rho_s)}{\sin a\Delta\rho} B_{\rho,0}. \tag{17}$$

The formulation of the suitable boundary value problem discussed here is a simple extension of the ideal-fluid thermocline theory discussed by Huang (1988). We also assume that along the eastern boundary water below the ventilated thermocline has a constant stratification,  $\rho_z^a = \text{const}$ , and PV in the unventilated thermocline is homogenized toward the northern boundary of the subtropical gyre (Rhines and Young 1982); that is, the PV for the stagnant water and the unventilated thermocline is

$$Q^a = -f\rho_z^a, \quad Q^h = -f_n\rho_z^a, \tag{18}$$

where  $f_n$  is the Coriolis parameter along the northern boundary of the subtropical gyre. As discussed by Huang (1988), the determination of the solution in the case with constant stratification for the unventilated thermocline and stagnant water is reduced to finding the depth of this  $\rho_0$  density surface.

Assuming that

$$B = B_0, \quad B_\rho = B_{\rho,0} \text{ at } \rho = \rho_0, \tag{19}$$

we obtain the following relations for the density layer below  $\rho_0$ :

$$B_\rho = B_{\rho,0} - fg(\rho - \rho_0)/Q^h, \tag{20}$$

$$B = B_0 + B_{\rho,0}(\rho - \rho_0) - fg(\rho - \rho_0)^2/2Q^h. \tag{21}$$

Along the eastern boundary where we assume that all ventilated isopycnals outcrop at  $z = 0$  (Luyten et al. 1983), the suitable boundary conditions are

$$B_e = 0, \quad B_{\rho,e} = 0 \text{ at } \rho = \rho_0. \tag{22}$$

Thus, the corresponding structure at the eastern boundary is

$$B_{\rho,e} = -fg(\rho - \rho_0)/Q^a, \tag{23}$$

$$B_e = z - fg(\rho - \rho_0)^2/2Q^a. \tag{24}$$

At the base of the moving water in the thermocline,  $\rho = \rho_b$ , both the Bernoulli function and its derivatives with respect to  $\rho$  should match with those for the stagnant water or for water along the eastern boundary; that is,

$$B = B_e, \quad B_\rho = B_{\rho,e} \text{ at } \rho = \rho_b. \tag{25}$$

Substituting (20) and (23) into (25) leads to

$$\rho_b - \rho_0 = -B_{\rho,0}Q^aQ^h/fg(Q^h - Q^a). \tag{26}$$

Substituting (26) into (20) leads to

$$B_{\rho,b} = B_{\rho,0}Q^h/(Q^h - Q^a). \tag{27}$$

Substituting (26) into (21) and (24) and using boundary condition (25) lead to

$$B_0 = B_{\rho,0}^2Q^aQ^h/2fg(Q^h - Q^a). \tag{28}$$

Let  $\rho = \rho_0$  in (16), substituting it into (28) leads to

$$B_{\rho,0} = \frac{2g(f_n - f)}{f_n\rho_z^a} \frac{\cos a\Delta\rho}{a \sin a\Delta\rho}. \tag{29}$$

The solution should satisfy another constraint, the Sverdrup constraint for a continuously stratified ocean. For the present case with uniform PV for the unventilated thermocline, the Sverdrup constraint is reduced to (Huang 1988)

$$B_{\rho,0}^3Q^h \frac{1 - (1 - f/f_n)^{-2}}{3fg} + \int_{\rho_s}^{\rho_0} B_\rho^2 d\rho = -\frac{2\rho_0f^2g}{\beta} \int_x^{x_e} w_e dx. \tag{30}$$

Using (17), the second term on the left-hand side of Eq. (30) is reduced to

$$\int_{\rho_s}^{\rho_0} B_\rho^2 d\rho = \frac{B_{\rho,0}^2}{a \sin^2 a\Delta\rho} \left( -\frac{1}{4} \sin 2a\Delta\rho + \frac{1}{2} a\Delta\rho \right). \tag{31}$$

Thus, Eq. (30) can be rewritten as

$$\begin{aligned}
& B_{\rho_0}^3 \frac{f_n \rho_z^a}{3fg} [1 - (1 - f/f_n)^{-2}] \\
& - \frac{B_{\rho_0}^2}{a \sin^2 a \Delta \rho} \left( -\frac{1}{4} \sin 2a \Delta \rho + \frac{1}{2} a \Delta \rho \right) \\
& = \frac{2\rho_0 f^2 g}{\beta} \int_x^{x_e} w_e dx. \quad (32)
\end{aligned}$$

Combining (29) and (32) leads to a single transcendental equation in the density difference  $\Delta \rho$ , the Coriolis parameter  $f$ , and the zonal position of the station  $x_e - x$ . Assuming that the Ekman pumping is independent of  $x$ , this equation is linear in  $x$ . Thus, for given  $f$  and  $\Delta \rho$  the zonal position of the station can be determined from this linear equation. This approach gives us the solution on an irregular grid in the  $x$  direction.

On the other hand, it is more desirable to calculate the solution on a regular grid; thus, for a given Ekman pumping forcing and the coefficient  $a_0$  in the PV function (11), the structure of the thermocline can be calculated by solving  $\Delta \rho$  from this nonlinear equation. It is readily seen that such a nonlinear equation may have multiple solutions. However, a solution for the thermocline structure in a closed basin also has to satisfy an additional constraint that the isopycnal depth should monotonically increase from zero on the sea surface to the depth of the  $\rho_0$  isopycnal surface. From Eq. (17), this means that a physically meaningful solution should satisfy the following constraint:

$$a \Delta \rho < \pi/2.$$

From our calculations, it was found that there is only one solution that can satisfy this additional constraint. The structure of the solution is controlled by the choice of several parameters, such as  $a_0$ ,  $\rho_z^a$ , and the others. From Eqs. (29) and (32), it is clear that along the eastern boundary  $a(\rho_0 - \rho_s) = \pi/2$  because the Ekman forcing term vanishes. Thus, we have a convenient relation to estimate parameter  $a_0$ :

$$a_0 = \frac{\pi}{2 \Delta \rho_e \sqrt{f_n g}},$$

where  $g$  is the gravitational acceleration, and  $\Delta \rho_e = \rho_0 - \rho_{s,e}$  is the density difference at the northeastern corner of the basin.

Note that this model requires that water with density  $\rho_0$  sink along the intergyre boundary. Similar to the case discussed by Huang (1988), near  $y = y_n$  (the northern boundary of the subtropical gyre) we have the following approximation:

$$\Delta \rho \propto \left( \frac{dw_e}{dy} \Delta x \right)^{-1/3}. \quad (33)$$

Therefore, the place where water with density  $\rho_0$ , that is,  $\Delta \rho = 0$ , is located at  $x = -\infty$ , along  $y = y_n$ .

### c. An example

The model has been applied to a model basin with geometry mimicking the North Atlantic:  $60^\circ \times 60^\circ$ ,  $a_0 = 1.234$  (assume  $\Delta \rho_e = 4\sigma$  units),  $\rho_z^a = -2.5 \times 10^{-8}$  (which corresponds to a density change of  $2.5 \sigma$  units over the depth of 1000 m), the Ekman pumping has a simple profile:

$$w_e = -1.0 \times 10^{-4} \sin \frac{y - y_s}{y_n - y_s} \text{ cm s}^{-1}.$$

The result shown below has a modest resolution of a regular  $101 \times 101$  grid.

The surface density distribution at lower latitudes is rather close to a zonal distribution; it has a northeastward tilt in the northern basin (Fig. 1a), rather similar to the surface density distribution in the North Atlantic. That the surface density pattern looks like the observed pattern is not a surprise because the assumption of a linear relation between potential thickness and the Bernoulli function is a good approximation. In fact, in the original ventilated thermocline model by Luyten et al. (1983) the potential thickness and the Bernoulli function for the upper layer have a linear relationship. Furthermore, the potential thickness functional relation, diagnosed from a model of the ideal-fluid thermocline in which the surface density is assumed to be purely zonal, is very close to a simple linear function with the coefficient almost independent of the density, as shown in Fig. 17 by Huang (1988). The density at the base of the wind-driven gyre (Fig. 1b) is somewhat too large, and this is probably due to our assumption of a constant potential thickness function for the unventilated thermocline. However, the depth of the wind-driven gyre (Fig. 1d) seems close to the solution based on more realistic parameters, as discussed by Huang (1990). At the sea surface the Bernoulli function is the same as the pressure; therefore Fig. 1c actually indicates the streamlines of an anticyclonic gyre on the sea surface.

In addition, we also include the circulation pattern on two isopycnal surfaces: the Bernoulli function (or the streamfunction on this isopycnal surface) and the depth of the isopycnal  $\sigma = 27.0$  are shown in Figs. 2a and 2b; and corresponding parts for  $\sigma = 23.8$  are shown in Figs. 2c and 2d. The first isopycnal  $\sigma = 27.0$  corresponds to the interface between the ventilated and unventilated thermocline in this case, so this isopycnal surface outcrops along the intergyre boundary. As discussed above, however, the surface density can reach this value only as  $x \rightarrow -\infty$ . At this time, it is unclear how to extend this solution into the subtropical region; thus, near the intergyre boundary the properties of this solution are not very clear. The second isopycnal surface outcrops along a curve in the northern basin, along which water is subducted and moves along the streamlines shown in Fig. 2c.

The structure of the thermocline is also shown through two zonal sections taken along  $y = 21^\circ \text{N}$  (Fig.

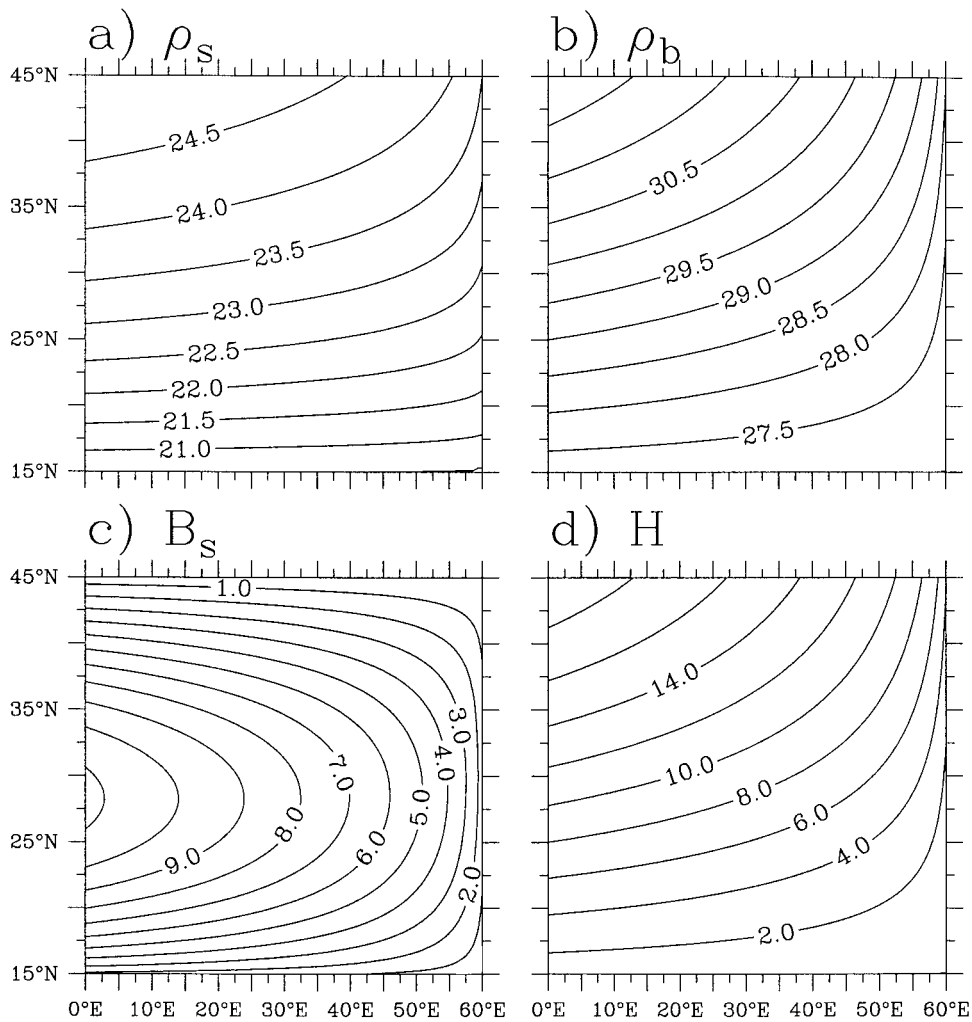


FIG. 1. The structure of the thermocline solution: (a) surface density in  $\sigma$  units; (b) density at the base of the wind-driven gyre, in  $\sigma$  units; (c) Bernoulli function on the sea surface, in units of  $0.1 \text{ kg m}^{-1} \text{ s}^{-2}$ ; and (d) the base of the wind-driven gyre, in 100 m.

3a), and  $y = 27^\circ\text{N}$  (Fig. 3b), and two meridional sections taken along  $x = 12^\circ\text{E}$  (Fig. 3c) and  $x = 54^\circ\text{E}$  (Fig. 3d). The horizontal curves in these figures indicate the stagnant water (or the so-called shadow zone in the original ventilated thermocline theory). Note that in this figure the isopycnal increment for the ventilated isopycnal layers is twice as big as that used in the unventilated layers. Thus, the stratification within the main thermocline is much higher than that in the unventilated thermocline or the stagnant water. In this figure and some other figures in this paper, we will focus on the upper part of the thermocline (800 m), so the lower part of the unventilated thermocline may not be included in these figures; however, the structure of the solution for this part of the thermocline can be inferred from the structure shown in these figures.

The only difference with the ideal-fluid thermocline solutions discussed by Luyten et al. (1983) and Huang (1988) is the lack of the pool region in the solution

discussed above. This is, however, not a substantial limitation because one can construct a solution whose PV function has any form specified a priori, as will be discussed shortly.

### 3. Solution with general forms of the potential thickness function

Note that the specific solution discussed above is the simplest possible solution. The basic formulation can be applied to the general case when the potential thickness is any given function of  $B$  and  $\rho$ ; that

$$B_{\rho\rho} = -fgD, \quad D = F(\rho, B), \quad (34)$$

where  $F(\rho, B)$  is a given function.

In particular, if we assume that

$$D = a_0^2[(1 + k^2) - 2k^2B^2]B,$$

the solution is in the form of Jacobi elliptical function

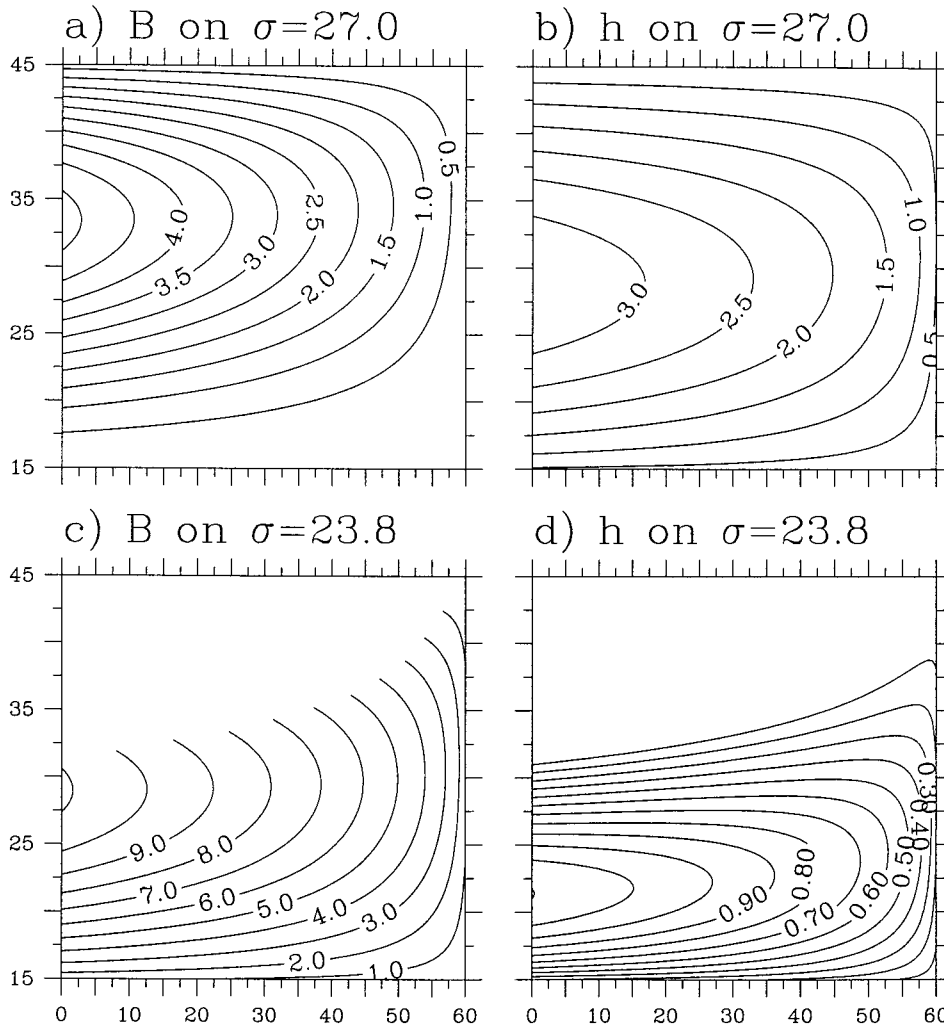


FIG. 2. Bernoulli function (streamfunction, in  $0.1 \text{ kg m}^{-1} \text{ s}^{-2}$ ) on two isopycnal surfaces (left panels), and the depth (in 100 m) of these isopycnal surfaces (right panels).

cn  $a(\rho - \rho_s, k)$ . This family of solutions is quite similar to the solution discussed above, so we will turn our attention to the general cases of  $D = F(\rho, B)$ . Similar to the case discussed in the main text, the structure of the ideal-fluid thermocline can be found by solving this equation subject to the following three constraints at each point  $(x, y)$  in the basin interior:

$$B_{\rho,0}^3 Q^h \frac{1 - (1 - f/f_n)^{-2}}{3fg} + \int_{\rho_s}^{\rho_0} B_\rho^2 d\rho = -\frac{2\rho_0 f^2 g}{\beta} \int_x^{x_e} w_e dx, \tag{35}$$

$$B_\rho = 0 \quad \text{at } \rho = \rho_s, \tag{36}$$

$$B_0 = -B_{\rho,0}^2 Q^a Q^h / 2fg(Q^a - Q^h) \quad \text{at } \rho = \rho_0. \tag{37}$$

Note that the upper boundary is free. This boundary value problem can be solved by a shooting method.

Assuming an initial guess for the depth of the  $\rho_0$  isopycnal surface, that is,  $B_\rho(\rho_0)$ , Eq. (34) can be integrated upward toward the surface (lower density), using a fourth-order Runge-Kutta scheme. The integration stops whenever  $B_\rho = 0$  and the density  $\rho_s$  where  $B_\rho(\rho_s) = 0$  is the surface density. By adjusting  $B_\rho(\rho_0)$ , a final solution can be found that satisfies all three constraints, including the most important dynamic constraint—the Sverdrup relation.

We show four examples here. The first two cases are produced by using a potential thickness function that depends on the density

$$D = a_0^2 B \xi(\rho), \tag{38}$$

where  $\xi(\rho)$  is a function of the density. For the first case, we assume a half-Gaussian profile

$$\xi(\rho) = 1 + 2 \exp\left[-\left(\frac{\rho_0 - \rho}{\Delta\rho}\right)^2\right], \quad \Delta\rho = 1.0. \tag{39}$$

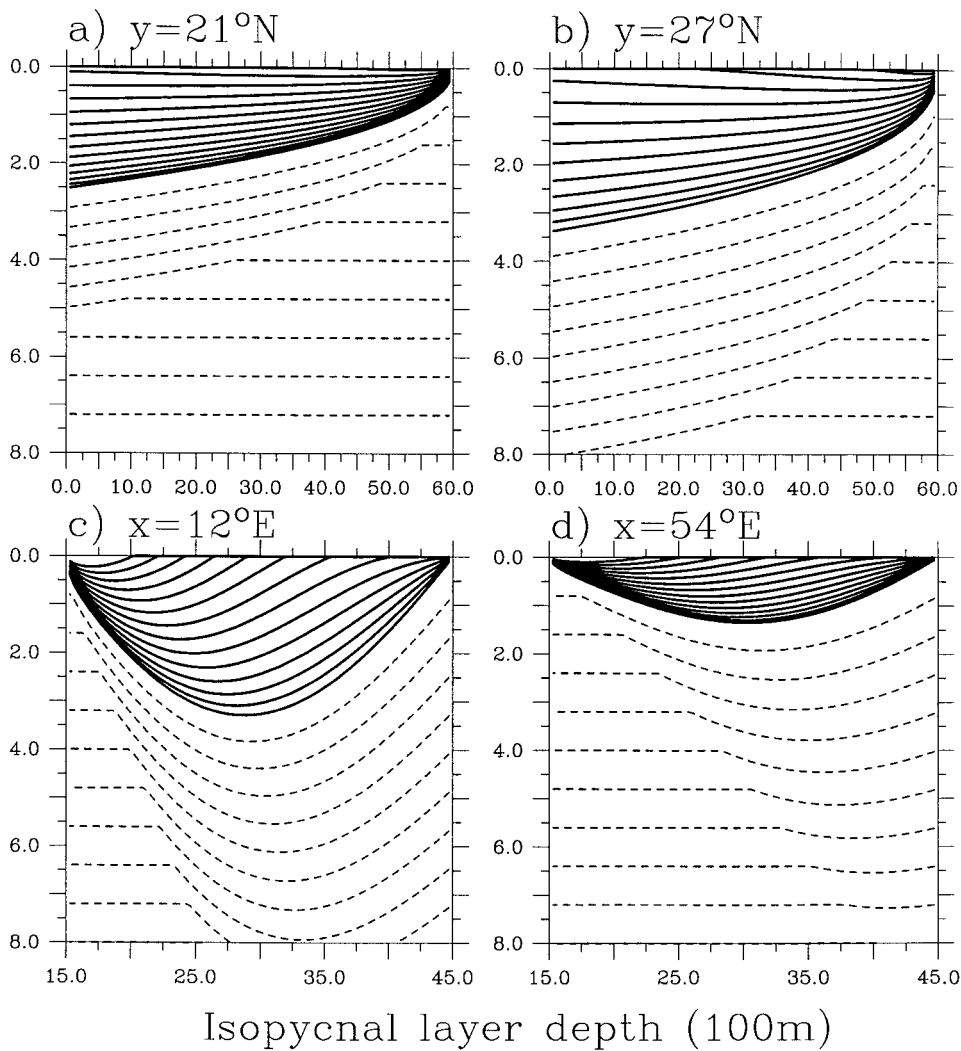


FIG. 3. Zonal sections and meridional sections through the model basin. Solid lines indicate the ventilated thermocline with an increment of  $\Delta\sigma = 0.4$ ; dashed lines depict the unventilated thermocline with an increment of  $\Delta\sigma = 0.2$ .

Using this function, we produce a subtropical gyre with a slightly higher density in the northern basin (Fig. 4a). Most interestingly, we have low PV for the first few ventilated layers, as shown in Fig. 4b. The potential thickness of layers with lighter density is gradually reduced. Of course, such PV structure is exactly what we specified above in the functional relation between potential thickness and density.

For the second example, we use a piecewise linear function of the density (in units of  $\sigma$ ):

$$\xi(\rho) = \begin{cases} 1 + 3(\rho_0 - \rho) & \text{if } \rho_0 - 1 < \rho < \rho_0 \\ 1 + 3(2 + \rho - \rho_0) & \text{if } \rho_0 - 2 < \rho < \rho_0 - 1 \\ 1 & \text{if } \rho < \rho_0 - 2. \end{cases} \quad (40)$$

This produces a low PV layer in the middle of the

ventilated layers (Fig. 5b), just as we expected from the functional relation specified above. Note that the low PV layer corresponds to a very low meridional surface density gradient in the northern basin, as shown in Fig. 5a.

We also explored the effect of nonlinearity associated with the Bernoulli function. Here we only show two simple cases. First, we assume that the potential thickness has a functional relation

$$D = a_0^2 B^{0.95}. \quad (41)$$

This functional relation produces a surface density pattern quite different from the previous cases. Most interestingly, the outcrop lines in the southeastern corner have a slightly NW–SE orientation, but in the northeastern basin, outcrop lines have a slightly SW–NE orientation (Fig. 6a). Note that such a pattern resembles

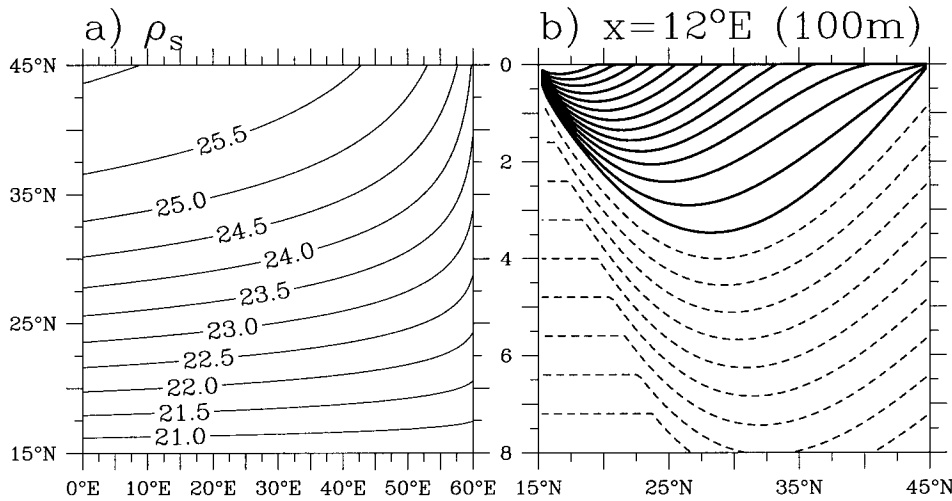


FIG. 4. Structure of the wind-driven circulation for the case with potential thickness in the form of a half Gaussian profile [Eq. (39)]. (a) The sea surface density; (b) a section through  $x = 12^\circ\text{E}$ , the solid lines indicate the ventilated thermocline, and the dashed lines the unventilated thermocline.

the sea surface density pattern in the North Pacific in late winter.

Second, we assume that the potential thickness function has the following form:

$$D = a_0^2 B^{1.1}. \tag{42}$$

This functional relation produces a circulation that is quite different from the previous case. The most interesting phenomenon is that sea surface density reaches a maximum south of the intergyre boundary, as shown in Fig. 7. In addition, the PV is much lower than that of the previous case.

#### 4. A Green function approach to climate variability induced by a buoyancy anomaly

##### a. Characteristic cone inferred from this model

An important application of this continuous solution of the ideal-fluid thermocline is the climate variability induced by a point source of Ekman pumping or buoyancy forcing. Due to the specific assumption about the functional relation between the potential thickness and Bernoulli function, it is rather difficult to infer the climate variability due to a surface forcing anomaly. A seemingly simple approach is to look at the difference between two solutions that correspond to a slightly dif-

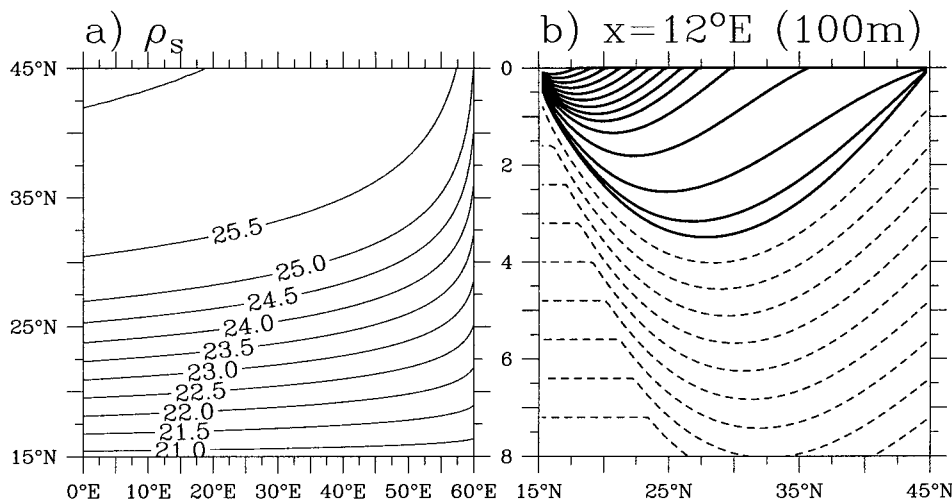


FIG. 5. Structure of the wind-driven circulation for the case with the potential thickness linearly dependent on the density: (a) the sea surface density and (b) a section through  $x = 12^\circ\text{E}$ ; the solid lines indicate the ventilated thermocline, and the dashed lines the unventilated thermocline.

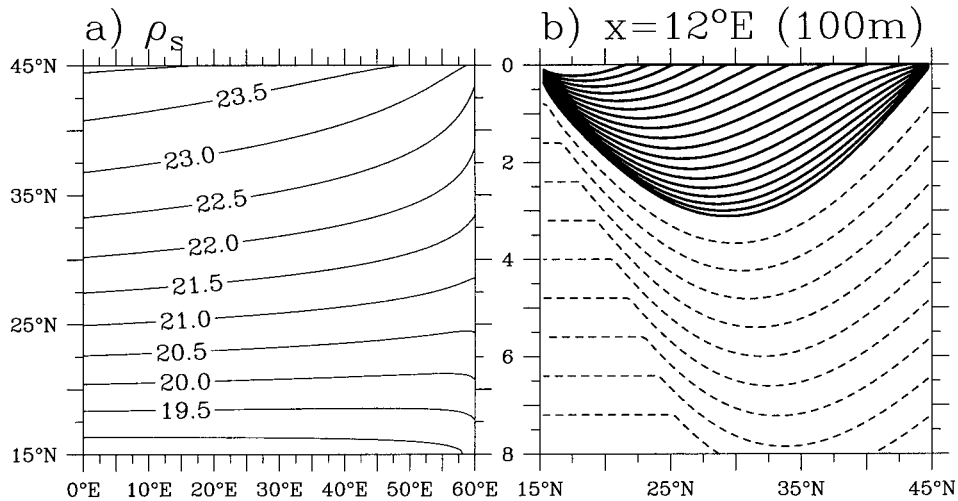


FIG. 6. Structure of the wind-driven circulation for the case with potential thickness function  $D = a_0^2 B^{0.95}$ : (a) the sea surface density and (b) a section through  $x = 12^\circ\text{E}$ ; the solid lines indicate the ventilated thermocline, and the dashed lines the unventilated thermocline.

ferent parameter  $a_0$ . However, this leads to a difference in buoyancy distribution over the entire basin, so this is not a very interesting solution. In the following we discuss the structure of perturbations induced by a point source of anomalous forcing.

First, if there is a point source of the Ekman pumping anomaly, there should be a response west of the perturbation because the Sverdrup relation involves a westward integration of the Ekman pumping. Since we have specified the functional relation between the potential thickness and the Bernoulli function, the perturbations inferred from the model are the following: West of the Ekman pumping anomaly, the surface density distribution is changed in such a way that the new surface

density distribution is consistent with the Ekman pumping pattern and the prespecified functional relation between potential thickness and the Bernoulli function. South of the perturbation latitude, however, there are no perturbations in the solution because the local solution should remain the same as before. Therefore, this model cannot be used to infer the climate variability due to a point source of Ekman pumping anomaly.

Second, if there is a point source of cooling or heating, the system should respond by creating a PV anomaly that propagates downstream within a characteristic cone, as discussed by Huang and Pedlosky (2000). For the case of a 20-ventilated-layer model, Huang (2000b) also showed the structure of the characteristic cone iden-

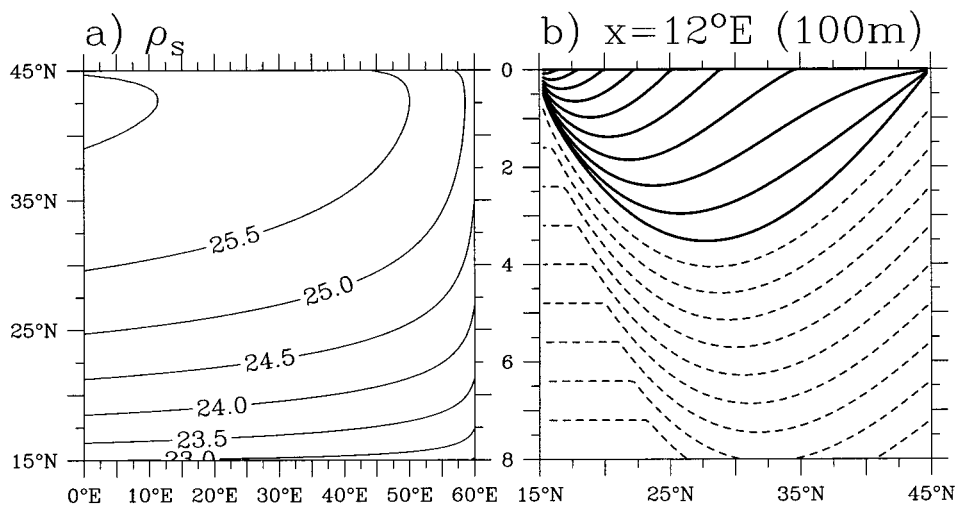


FIG. 7. Structure of the wind-driven circulation for the case with the potential thickness function  $D = a_0^2 B^{1.1}$ : (a) the sea surface density and (b) a section through  $x = 12^\circ\text{E}$ ; the solid lines indicate the ventilated thermocline, and the dashed lines the unventilated thermocline.

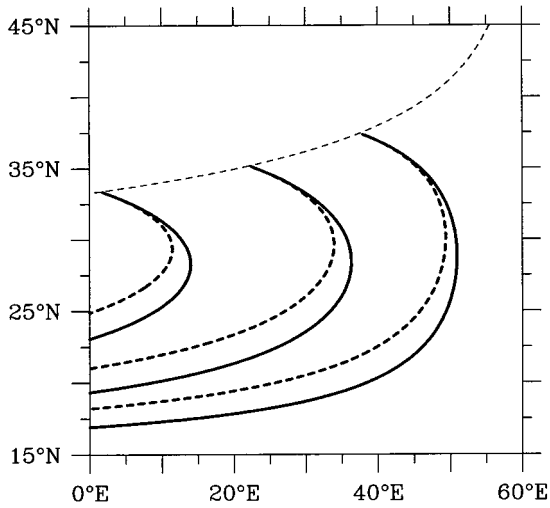


FIG. 8. Characteristic cones stemming from perturbations located along the isopycnal outcrop line ( $\sigma = 24.0$ ), indicated by the thin dashed line. The eastern edges of the cones are defined by the streamlines on the sea surface and indicated by the heavy solid lines. The western edges of the cones are defined by the streamlines on the  $\sigma = 24.0$  isopycnal surface (heavy dashed lines).

tified from the numerical solution. In the present case, however, such characteristic cones can be constructed from the truly continuous solution. An example is shown in Fig. 8: along the outcrop line of  $\sigma = 24.0$  (depicted by the thin dashed line) a cooling anomaly induces a potential thickness anomaly that propagates southwestward along a streamline on isopycnal  $\sigma = 24.0$ . This streamline serves as the western edge of the characteristic cone. Since this isopycnal is subducted, the streamline is depicted by a heavy dashed line. This streamline carries the primary potential thickness anomaly, along whose path a secondary potential thickness anomaly is created whenever this primary characteristic crosses a new outcrop line. The newly created secondary potential thickness anomaly propagates on the corresponding new isopycnal. This secondary potential thickness anomaly in turn creates a tertiary potential thickness anomaly, which gives rise to a potential thickness anomaly of higher order, and so on. As discussed by Huang and Pedlosky (2000), the eastern edge of the characteristic cone is defined by the streamline on the sea surface (which is represented by a constant Bernoulli function contour line) that passes through the point source of buoyancy anomaly, as depicted by solid lines in Fig. 8. Therefore, the eastern and western edges of the characteristic cone can be defined by the streamlines on the

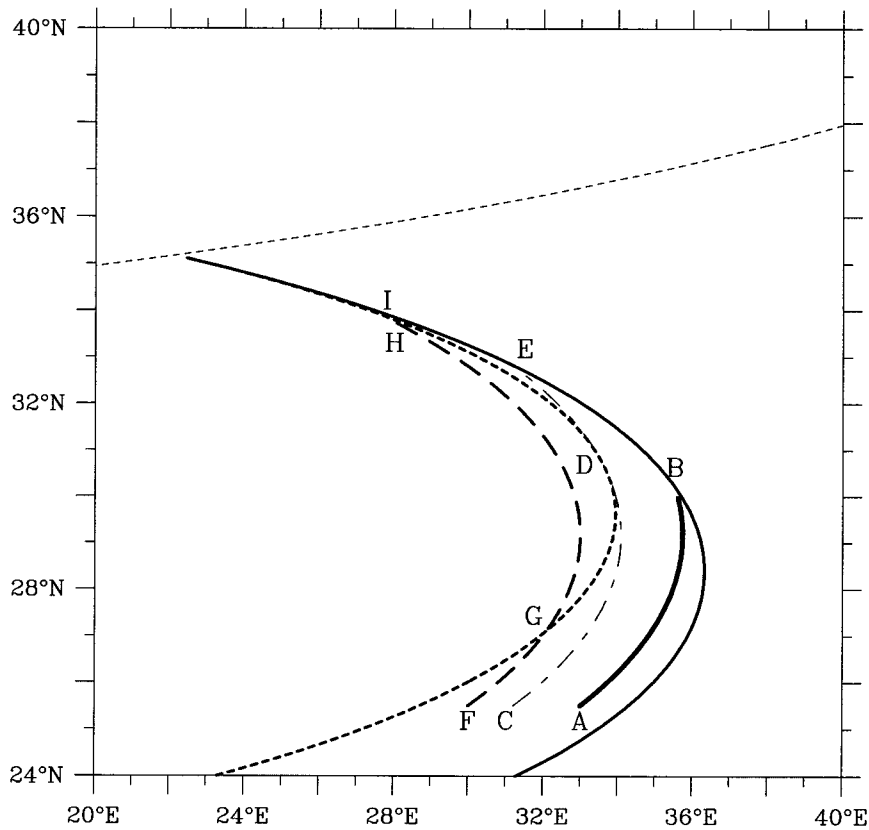


FIG. 9. Domain of dependence for three stations A (AB), C (CDE), and F (FGHI) within the characteristic cone stemming from a point source of perturbation, see text for details.

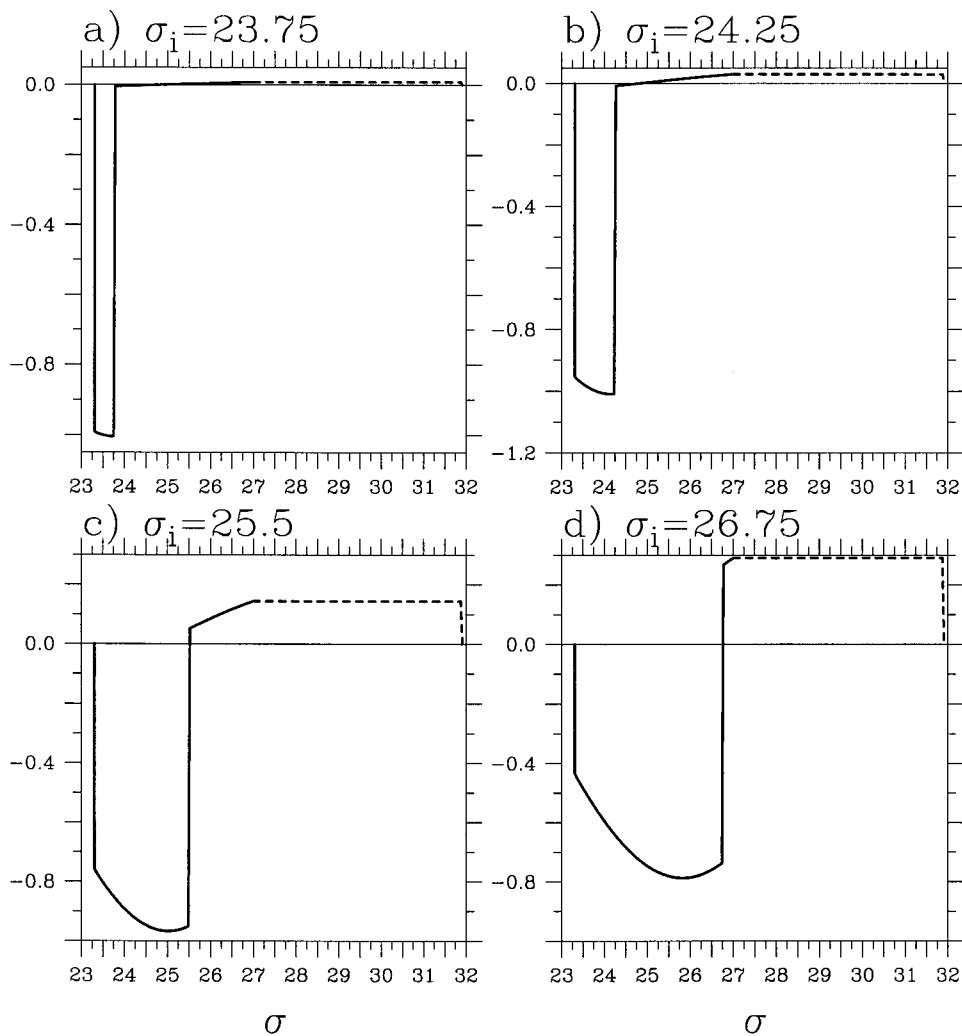


FIG. 10. The first derivative of the Green function (taken for a station at the center of the basin) for PV anomaly input at different densities  $\rho_i$ .

sea surface and on the isopycnal surface  $\sigma = 24.0$ , respectively.

The characteristic cone discussed above defines the so-called domain of influence for a point source, that is, the region downstream that is influenced by this point source of anomaly. Due to the velocity shear in the vertical direction, the characteristic cone becomes wider and wider downstream. Within the cone, however, the solution at an individual station depends on the PV function that is set up from the upstream condition; that is, the solution at each station is controlled by the condition within the so-called domain of dependence. Similar to the domain of influence, the domain of dependence gradually expands in the upstream direction. The solution at each station can be determined by tracing upstream along characteristics and finding out the PV anomaly advected along characteristics passing through the station.

In the present case, all PV anomalies are set up at the outcrop lines by a subsurface PV anomaly that is advected from upstream. In order to find the PV anomaly at a given density  $\rho_i$  that passes through a given station, one can follow a search procedure: first, use (16) to calculate the Bernoulli function  $B_i$  for the density  $\rho_i$  at the subsurface depth; second, find the location  $(x, y)$  by matching both  $B_i$  and  $\rho_i$  with the Bernoulli function and density on the upper surface obtained from the unperturbed solution. The whole domain of dependence for stations within the characteristic cone can be defined through this search procedure. As an example, the domains of dependence for three stations, A, C, and F, within the characteristic cone are shown in Fig. 9. The solution at station A depends on the PV anomaly set up along line AB. Note that surface density increases from A to B. (The streamline connecting points A and B on the isopycnal surface that outcrops at point B is omit-

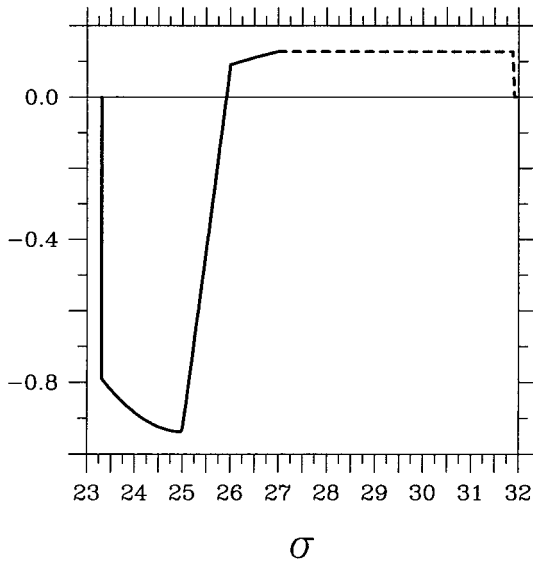


FIG. 11. The first derivative of the Green function for PV anomaly input  $25 \leq \sigma \leq 26$ .

ted.) Similarly, the solution at C depends on the PV anomaly set up along line CDE, and the solution at F depends on the PV anomaly set up along line FGHI.

However, line CDE represents a critical situation because it is tangential to the western edge of the characteristic cone at point D where the two segments, CD and DE, join. For the solution at F, the uppermost segment corresponding to DE shrinks to a tiny segment HI that is within the characteristic cone and represents the PV perturbation influence on a deep density segment. The segment GH is outside the characteristic cone. As

a result, there is no PV perturbation signal coming within this density range. Slightly upward in the water column, the PV perturbation signal comes again from the density corresponding to segment FI.

Therefore, for the present case, west of station C, the perturbation solution at a station may have PV anomalies entering the water column at two density intervals, one below the surface and the second one farther below in the water column.

Although we have identified the edge of the characteristic cone, the exact structure of the perturbation within this cone remains a theoretical challenge. As discussed above, there are many characteristics within this cone, and at each station within the cone the exact form of the perturbation depends on the combined effect of all these potential thickness perturbations. A four-layer model discussed by Huang and Pedlosky (2000) provides a glimpse of the complexity. As the number of outcrop lines increases, the number of the characteristics grows exponentially. Thus, the structure of the characteristic cone in a multilayer model or a continuous model may be another example of the exponential explosion of the complexity. Until a better approach is found to overcome this complexity, our discussion is limited to the western edge of this characteristic cone, where there is only a single characteristic involved.

*b. Green function*

Climate variability induced by a point source of perturbation can be understood better in terms of the Green function as follows. Assume that a single PV perturbation will affect the solution in the following manner:

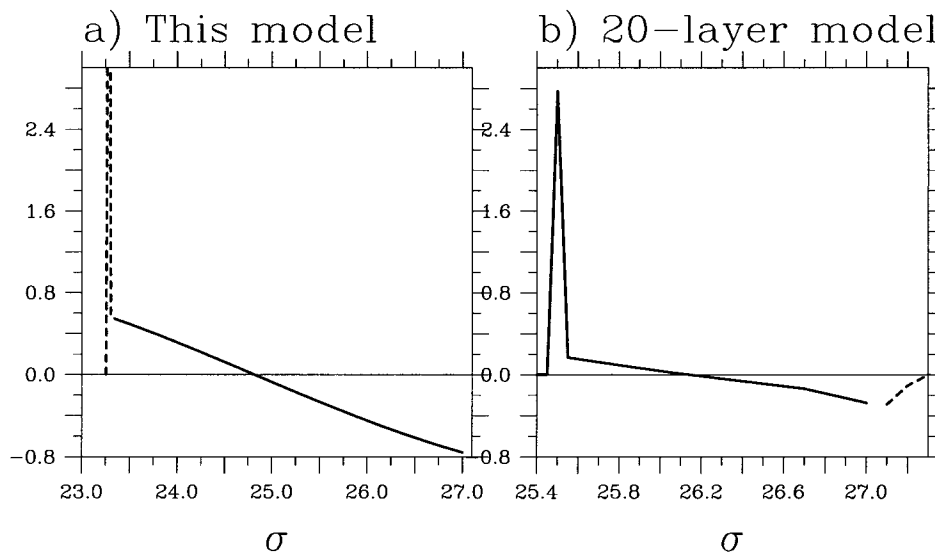


FIG. 12. Green functions representing the system's response to a surface density anomaly. (a) Result from this model; the dashed line on the left end indicates a surface-trapped  $\delta$ -function response. (b) Result from model with 20 ventilated layers, plus a mixed layer and the unventilated thermocline (Huang 2000b). The dashed line indicates the perturbation within the unventilated thermocline.

$$\delta B_{\rho\rho} + a^2 \delta B = d \cdot \delta(\rho - \rho_i) + \Delta \cdot \delta(\rho - \rho_1), \quad (43)$$

where  $\rho_i$  is the density layer where the PV perturbation (its strength is  $d$ ) enters the water column, and we will assume  $\rho_i$  satisfies the constraint:  $\rho_s < \rho_i < \rho_0$ . The second term on the right-hand side denotes the possible PV perturbation for the uppermost density layer. Recall that the model assumes a specified potential thickness function, so the surface density under the perturbed boundary condition may be different from  $\rho_s$  in the unperturbed solution. This perturbation is due to changes in the circulation, so that PV for the uppermost layer may not satisfy the same relation  $D = a_0^2 B$ , as specified a priori.

We seek the solution in terms of the Green function. For the present case, the Green function is

$$\delta B^- = c_1 \cos a(\rho - \rho_1), \quad \text{for } \rho_s < \rho < \rho_i, \quad (44)$$

$$\delta B_\rho^- = -ac_1 \sin a(\rho - \rho_1), \quad \text{for } \rho_s < \rho < \rho_i, \quad (45)$$

$$\delta B^+ = c_2 \cos a(\rho - \rho_2) \quad \text{for } \rho_i < \rho < \rho_0, \quad (46)$$

$$\delta B_\rho^+ = -ac_2 \sin a(\rho - \rho_2), \quad \text{for } \rho_i < \rho < \rho_0. \quad (47)$$

There are five unknown constants:  $\rho_1$ ,  $\rho_2$ ,  $c_1$ ,  $c_2$ , and  $\Delta$ . In order to determine these constants, we need the following five constraints:

1) Continuity of  $\delta B$  at  $\rho_i$ : This constraint leads to

$$c_2 = \frac{\cos a(\rho_i - \rho_1)}{\cos a(\rho_i - \rho_2)} c_1. \quad (48)$$

2) Integrating Eq. (43) over the density range  $[\rho_i - \delta\rho, \rho_i + \delta\rho]$  and letting  $\delta\rho \rightarrow 0$ , we have the jump condition

$$\delta B_\rho^+ - \delta B_\rho^- = d, \quad \text{at } \rho = \rho_i. \quad (49)$$

Thus, we have a relation

$$-c_2 a \sin(\rho_i - \rho_2) + c_1 a \sin a(\rho_i - \rho_1) = d. \quad (50)$$

Combining (48) and (50) leads to

$$c_1 = \frac{d \cos a(\rho_i - \rho_2)}{a \sin a(\rho_2 - \rho_1)}, \quad (51)$$

$$c_2 = \frac{d \cos a(\rho_i - \rho_1)}{a \sin a(\rho_2 - \rho_1)}. \quad (52)$$

3) Integrating Eq. (43) across the upper boundary  $\rho_s$  leads to

$$-c_1 a \sin a(\rho_s - \rho_1) = \Delta/2. \quad (53)$$

This relation will be used to determine the PV perturbation for the uppermost layer, which is subducted at this station.

4) As discussed above, at the  $\rho_0$  isopycnal surface Eq. (28) provides another constraint. Taking the perturbation of (28) leads to

$$\delta B = \frac{f_n \rho_z^a}{g(f - f_n)} B_{\rho,0} \delta B_\rho \quad \text{at } \rho = \rho_0 \quad (54)$$

so that

$$\tan a(\rho_0 - \rho_2) = -\frac{g(f - f_n)}{a f_n \rho_z^a B_{\rho,0}}. \quad (55)$$

Using (29), this leads to

$$\tan a(\rho_0 - \rho_2) = \frac{1}{2} \tan a(\rho_0 - \rho_s). \quad (56)$$

Thus, we have a simple relation that  $\rho_2$  is roughly half way between  $\rho_s$  and  $\rho_0$ . From (47), it is readily seen that for the case when  $\rho_i < \rho_2$ , the lower branch of the Green function should have a zero-crossing at  $\rho_2$ .

5) The Sverdrup constraint (30) leads to a constraint for the perturbations

$$B_{\rho,0}^2 \frac{f_n \rho_z^a}{fg} [1 - (1 - f/f_n)^{-2}] \delta B_{\rho,0} - 2 \int_{\rho_s}^{\rho_0} B_\rho \delta B_\rho d\rho = 0. \quad (57)$$

After some algebraic manipulations, this leads to

$$B_{\rho,0} \sin a(\rho_0 - \rho_2) \sin a(\rho_0 - \rho_s) \frac{f_n \rho_z^a}{fg} [1 - (1 - f/f_n)^{-2}] = \frac{\cos a(\rho_i - \rho_2)}{\cos a(\rho_i - \rho_1)} \left[ -\frac{1}{2a} \sin a(2\rho_i - \rho_s - \rho_1) + \frac{1}{2a} \sin a(\rho_a - \rho_1) + (\rho_i - \rho_s) \cos a(\rho_1 - \rho_s) \right] + \left[ -\frac{1}{2a} \sin a(2\rho_0 - \rho_s - \rho_2) + \frac{1}{2a} \sin a(2\rho_i - \rho_s - \rho_2) + (\rho_0 - \rho_i) \cos a(\rho_2 - \rho_s) \right]. \quad (58)$$

Because this is a perturbation to the existing solution at a given station,  $\rho_s$  is known from the unperturbed

solution at this station. Using relations (51), (52), and (56), Eq. (58) is reduced to a nonlinear algebraic equation for a single variable  $\rho_1$ , which can be solved nu-

merically. The structure of the solution can be found accordingly.

*c. Perturbations due to surface cooling/heating*

In this section we discuss the case of a surface density anomaly. We also assume that there is no source of PV perturbation below the surface density layer, so the Green function can be written as

$$\delta B = C \cos a(\rho - \rho_2), \tag{59}$$

and its first derivative is

$$\delta B_\rho = -aC \sin a(\rho - \rho_2), \tag{60}$$

where  $C$  and  $\rho_2$  are constants to be determined from the following two constraints:

1) Similar to the discussion above, at the lower boundary the variation of (28) leads to a constraint (56), which determines  $\rho_2$ . As discussed above, this relation means that the Green function should have a zero-crossing at  $\rho_2$ . That surface density anomaly can induce second baroclinic modes or other high internal modes can be shown clearly by taking the variation of the Sverdrup constraint, as discussed by Huang and Pedlosky (2000).

2) The additional constraint can be obtained by taking the variation of the Sverdrup constraint (30). The first term on the left-hand side of (30) leads to

$$-aC \sin a(\rho_0 - \rho_2) B_{\rho_0}^2 \frac{f_n \rho_s^a}{fg} [1 - (1 - f/f_n)^{-2}]. \tag{61}$$

The second term on the left-hand side of (29) is reduced to

$$2 \int_{\rho_s}^{\rho_0} B_\rho \delta B_\rho d\rho - B_\rho^2(\rho_s) \delta \rho_s = I_1 + I_2, \tag{62}$$

$$I_1 = \frac{aCB_{\rho_0}}{\sin a\Delta\rho} \left[ \frac{1}{2a} \sin a(2\rho_0 - \rho_s - \rho_2) + \frac{1}{2a} \sin a(\rho_2 - \rho_s) - \cos a(\rho_2 - \rho_s)(\rho_0 - \rho_s) \right], \tag{63}$$

$$I_2 = - \left[ \frac{B_{\rho_0}}{\sin a\Delta\rho} \sin a\delta\rho_s \right]^2 \delta\rho_s \approx - \frac{B_{\rho_0}^2}{\sin^2 a\Delta\rho} a^2 \delta\rho_s^3. \tag{64}$$

Thus, the Sverdrup constraint is finally reduced to

$$(X + Y)C = \frac{aB_{\rho_0}}{\sin a\Delta\rho} \delta\rho_s^3, \tag{65}$$

where

$$X = B_{\rho_0} \sin a\Delta\rho \sin a(\rho_0 - \rho_2) \frac{f_n \rho_s^a}{fg} [1 - (1 - f/f_n)^{-2}],$$

$$Y = \frac{1}{2a} \sin a(2\rho_0 - \rho_s - \rho_2) + \frac{1}{2a} \sin a(\rho_2 - \rho_s) - \cos a(\rho_2 - \rho_s)(\rho_0 - \rho_s).$$

Note that  $X$  represents the contribution due to the unventilated thermocline, thus  $|X| > |Y|$ . Thus the sign of  $X + Y$  is controlled by  $X$ . From Eq. (65),  $\delta\rho_s$  and  $C$  should have the same sign. For example, due to surface cooling, density increases; that is,  $\delta\rho_s > 0$  and  $C > 0$ . Accordingly, we have

$$\delta B_\rho > 0 \quad \text{for } \rho_s < \rho < \rho_2,$$

$$\delta B_\rho < 0 \quad \text{for } \rho_2 < \rho < \rho_0.$$

Therefore, surface cooling induces an upward motion in the upper part of the thermocline and a downward motion in the lower part of the thermocline. This is consistent with the results from both a multiple-layer model (Huang and Pedlosky 1999) and a continuously stratified model by Huang (2000b).

The structure of the Green function representing the response of the system (at a station exactly in the center of the model basin) to a subsurface PV anomaly is shown in Fig. 10, with  $d = 1$ , that is, a positive PV anomaly (corresponding to surface heating). Instead of the Green function itself, here we show its first derivative ( $\delta B_\rho$ ) because it corresponds to the vertical displacement of the isopycnal. Since this Green function satisfies the condition of a depth-weighted zero integration, its amplitude is larger at shallow levels. In particular, if the forcing is very close to the surface, the Green function looks like a surface-trapped  $\delta$  function, as shown in Fig. 10a. As the PV input moves down to the lower part of the thermocline, the response in the lower part of the water column becomes larger. In addition, the system possesses an eigenmode, which has a zero crossing,  $\sigma_2$ , as shown in (47). For the station discussed here, it is located at  $\sigma_2 = 24.81$ . Thus, if  $\sigma_i < \sigma_2$ , the Green function has a zero-crossing at  $\sigma_2$ , as shown in Figs. 10a and 10b. On the other hand, if  $\sigma_i > \sigma_2$ , the zero-crossing is located at the jump point  $\sigma_i$ , as shown in Figs. 10c and 10d.

Note that the Green function discussed here is defined for  $\rho > \rho_0$  only. Since we assume that PV of the unventilated thermocline is homogenized, the corresponding change in  $B_\rho$  is constant for the density range  $\rho_0 < \rho < \rho_b$ . The dashed lines in Fig. 10 depict this extrapolation of the Green function to the unventilated thermocline.

The Green function for the present case has a prominent structure in the form of the so-called second dynamic thermocline mode, as discussed by Huang and Pedlosky (2000). However, note that we do not rule out the possibility that higher modes can exist because our

results obtained here belong to a special family of thermocline solutions.

In reality, the PV anomaly input appears over a finite density range, so the response of the system to such anomalous forcing is smoothed. For example, at the same station (in the middle of the basin) the Green function averaged over the uniform input within the density range of  $25 \leq \sigma \leq 26$  has a continuous transition between the positive and negative parts, as shown in Fig. 11. If the PV input is not uniform within this density range, the resulting Green function may have quite a different shape.

The Green function induced by a point source of cooling is in the form of a surface-trapped  $\delta$  function (Fig. 12a). This solution is calculated at the center of the basin. Note that this solution is consistent with the structure of the Green function shown in Fig. 10. As  $\rho_i$  approaches sea surface density, the corresponding Green function becomes more and more  $\delta$ -function-like. This solution is consistent with the perturbation solution calculated from a model with 20 ventilated thermocline layers (Fig. 12b), including a mixed layer and the unventilated thermocline, as discussed by Huang (2000b). This solution is produced by moving the 15th outcrop line ( $\sigma = 25.5$ ) northward by  $dy = 0.01^\circ$ ; the solution shown here is taken at  $40^\circ\text{E}$  (the basin is within  $0^\circ$ – $60^\circ\text{E}$ ).

## 5. Conclusions

We have shown that the structure of wind-driven circulation in the subtropical basins, or the thermocline, can be simulated by specifying simple functional relations for the potential thickness. Assuming a linear function such as  $D = a_0^2 B$  for the ventilated thermocline and a constant potential thickness for the unventilated thermocline gives rise to a solution that resembles the subtropical gyres observed in the oceans. Note that Welander's solution is based on the potential thickness function

$$D = \frac{1}{\alpha\rho + \beta B + \gamma}$$

for all density layers. In addition, his solution does not satisfy the Sverdrup constraint, but our new solution does satisfy the Sverdrup constraint. The differences between Welander's formulation and our new formulation are dynamically critical, and they reflect a much deeper physical understanding of the thermocline problem than in the past.

It was unclear from previous studies what might happen when the number of ventilated layers in the ideal-fluid thermocline theory goes to infinity. Is a truly continuous solution possible? Or might the solution appear in the form of a density discontinuity in the otherwise truly continuous model? We have shown that such a density front is not necessary in the continuous limit of the ideal-fluid thermocline. In fact, we have presented

a simple solution that has a truly continuous structure in three-dimensional space, including a weak discontinuity in PV at the interface between the ventilated and unventilated thermoclines.

It is important to emphasize that this continuous solution is obtained under the assumption that PV is uniform for the unventilated thermocline. The nonexistence of the PV singularity in the unventilated thermocline implies a finite rate of mixing that sets up such a PV relation in the unventilated thermocline in the basin. In fact, the dynamic roles of diapycnal mixing, horizontal mixing, and recirculation have been implicitly included through the specification of the PV of the unventilated thermocline in the ideal-fluid thermocline theory.

On the other hand, it is quite straightforward to produce an ideal-fluid thermocline solution with step-function-like discontinuity in density. Using a one-dimensional model, which represents a balance between vertical advection and diffusion, one can easily generate the PV functional relation for the unventilated thermocline. As diffusion is gradually weakened, a sharp internal density (or PV) front appears in the unventilated thermocline. Given such a PV functional relation with a relatively sharp internal front, the ideal-fluid thermocline model can give rise to a solution that further enhances the density gradient across such a front and produces a step-function-like main thermocline, see Fig. 4 by Huang (2000a). This solution resembles the sharp thermocline produced by a numerical model with weak vertical mixing by Samelson and Vallis (1997). Therefore, within the theoretical framework of the ideal-fluid thermocline, it is possible to generate solutions with or without internal density discontinuity, and these solutions are idealizations of the wind-driven circulation under different conditions or theoretical limits.

The climate variability due to a point source of cooling or heating remains unclear. It is speculated that this problem can be reduced to the construction of the Green function, which may involve integrating the perturbations into a unified structure. It is possible that the exponential explosion of the characteristics may be overcome by some transformation of coordinates or variables. I have attempted to reveal the structure of the Green function corresponding to a point source of cooling/heating. However, it remains unclear how to find the complete structure of the Green function for the point source of anomalous buoyancy forcing.

*Acknowledgments.* It is a pleasure to thank my colleague Joe Pedlosky for his interest and encouragement during my long-time pursuit of the ideal-fluid thermocline solutions. Reviewers' comments and B. Gaffron's careful editing helped to improve the presentation of the materials. This study was supported by a Mellon Independent Study Award and the National Science Foundation through Grant OCE-9616950 to the Woods Hole Oceanographic Institution. This paper is dedicated to the memory of the pioneers of the thermocline theory:

Pierre Welander on the 75th anniversary of his birth and Hank Stommel on the 80th anniversary of his birth; their profound influence has been a continuous source of inspiration.

## REFERENCES

- Deser, C., M. A. Alexander, and M. S. Timlin, 1996: Upper ocean thermal variability in the North Pacific during 1970–1991. *J. Climate*, **9**, 1840–1855.
- Hood, S., and R. Williams, 1996: On frontal and ventilated models of the main thermocline. *J. Mar. Res.*, **54**, 211–238.
- Huang, R. X., 1986: Solutions of the ideal fluid thermocline with continuous stratification. *J. Phys. Oceanogr.*, **16**, 39–59.
- , 1988: On boundary value problems of the ideal-fluid thermocline. *J. Phys. Oceanogr.*, **18**, 619–641.
- , 1990: On the three-dimensional structure of the wind-driven circulation in the North Atlantic. *Dyn. Atmos. Oceans*, **15**, 117–159.
- , 1991: The three-dimensional structure of wind-driven gyres: Ventilation and subduction. *U.S. National Report to International Union of Geodesy and Geophysics 1987–1990 Supplement to Rev. Geophys.*, 590–609.
- , 2000a: Parameter study of a continuously stratified model of the ideal-fluid thermocline. *J. Phys. Oceanogr.*, **30**, 1372–1388.
- , 2000b: Climate variability inferred from a continuously stratified model of the ideal-fluid thermocline. *J. Phys. Oceanogr.*, **30**, 1389–1406.
- , and J. Pedlosky, 1999: Climate variability inferred from a layered model of the ventilated thermocline. *J. Phys. Oceanogr.*, **29**, 779–790.
- , and —, 2000: Climate variability induced by anomalous forcing in a multilayer model of the ventilated thermocline. *J. Phys. Oceanogr.*, **30**, 3009–3021.
- Killworth, P. D., 1987: A continuously stratified nonlinear ventilated thermocline. *J. Phys. Oceanogr.*, **17**, 1925–1943.
- Liu, Z., 1999: Forced planetary wave response in a thermocline gyre. *J. Phys. Oceanogr.*, **29**, 1036–1055.
- Luyten, J., J. Pedlosky, and H. M. Stommel, 1983: The ventilated thermocline. *J. Phys. Oceanogr.*, **13**, 292–309.
- Pedlosky, J., 1996: *Ocean Circulation Theory*. Springer, 453 pp.
- , and P. Robbins, 1991: The role of finite mixed-layer thickness in the structure of the ventilated thermocline. *J. Phys. Oceanogr.*, **21**, 1018–1931.
- Rhines, P. B., and W. R. Young, 1982: A theory of the wind-driven circulation. I. Mid-ocean gyres. *J. Mar. Res.*, **40**(Suppl.), 559–596.
- Robinson, A. R., and H. Stommel, 1959: The oceanic thermocline and the associated thermohaline circulation. *Tellus*, **11**, 295–308.
- Salmon, R., 1990: The thermocline as an “internal boundary layer.” *J. Mar. Res.*, **48**, 437–469.
- Samelson, R. M., and G. K. Vallis, 1997: Large-scale circulation with diapycnal diffusion: The two-thermocline limit. *J. Mar. Res.*, **55**, 223–275.
- , and R. Hollerbach, 1991: Similarity solutions of the thermocline equations. *J. Mar. Res.*, **49**, 249–280.
- Schneider, N., A. J. Miller, M. A. Alexander, and C. Deser, 1999: Subduction of decadal North Pacific temperature anomalies: Observations and dynamics. *J. Phys. Oceanogr.*, **29**, 1056–1070.
- Vallis, G. K., 2000: Large-scale circulation and production of stratification: Effects of wind, geometry and diffusion. *J. Phys. Oceanogr.*, **30**, 933–954.
- Veronis, G., 1969: On theoretical models of the ocean thermocline circulation. *Deep-Sea Res.*, **16**(Suppl.), 301–323.
- Welander, P., 1959: An advective model of the ocean thermocline. *Tellus*, **11**, 309–318.
- , 1971: Some exact solutions to the equation describing an ideal fluid thermocline. *J. Mar. Res.*, **29**, 60–68.
- Williams, R. G., 1991: The role of the mixed layer in setting the PV of the main thermocline. *J. Phys. Oceanogr.*, **21**, 1803–1814.